The Astrophysical Journal, 918:49 (11pp), 2021 September 10 https://doi.org/10.3847/1538-4357/ac0e37

Improved Methods for Estimating Peculiar Velocity Correlation Functions Using Volume Weighting

Yuyu Wang[1,2], Sarah Peery[3], Hume A. Feldman[2], and Richard Watkins[3]
[1] Department of Astronomy, School of Physics and Astronomy, Shanghai Jiao Tong University, Shanghai, 200240, People's Republic of China
yuyuwang@sjtu.edu.cn
[2] Department of Physics & Astronomy, University of Kansas, Lawrence, KS 66045, USA
[3] Department of Physics, Willamette University, Salem, OR 97301, USA
Received 2020 October 23; revised 2021 June 17; accepted 2021 June 22; published 2021 September 7

Abstract

We present an improved method for calculating the parallel and perpendicular velocity correlation functions directly from peculiar velocity surveys using weighted maximum-likelihood estimators. A central feature of the new method is the use of a position-dependent weighting scheme that reduces the influence of nearby galaxies, which are typically overrepresented relative to more distant galaxies in most surveys. We demonstrate that correlation functions calculated in this way are less susceptible to biases due to our particular location in the universe, and thus are more easily comparable to linear theory and between surveys. Our results suggest that the parallel velocity correlation function is a promising cosmological probe, given that it provides a better approximation of a Gaussian distribution than other velocity correlation functions and that its bias is more easily minimized by weighting. Though the position-weighted parallel velocity correlation function increases the statistical uncertainty, it decreases the cosmic variance and is expected to provide more stable and tighter cosmological parameter constraints than other correlation methods in conjunction with more precise velocity surveys in the future.

Unified Astronomy Thesaurus concepts: Cosmology (343)

1. Introduction

Studies of density perturbations provide information used to analyze the large-scale structure of the universe. However, density perturbation studies based on galaxy redshift distributions are limited by the bias due to peculiar velocities, also known as redshift space distortion (RSD). Many studies have shown the effects of peculiar velocities in RSD studies (e.g., Kaiser 1987; Melott et al. 1998; Scoccimarro 2004; Thomas et al. 2004; Taruya et al. 2010; Reid & White 2011; Seljak & McDonald 2011; Song et al. 2013; Taruya et al. 2013; Zhang et al. 2013; Zheng et al. 2013; Senatore & Zaldarriaga 2014; Okumura et al. 2015; Uhlemann & Kopp 2015; Bianchi et al. 2016; Vlah et al. 2016; Hand et al. 2017; Bel et al. 2019).

Peculiar velocity is a powerful tracer of mass distribution (e.g., Watkins et al. 2009; Feldman et al. 2010; Davis et al. 2011; Macaulay et al. 2011; Nusser et al. 2011; Macaulay et al. 2012; Turnbull et al. 2012; Johnson et al. 2014; Nusser 2014; Springob et al. 2014; Scrimgeour et al. 2016). However, current peculiar velocity measurements are still based on radial distances, which limit the precision of peculiar velocity surveys. A different method of measuring peculiar velocity can be performed using the kinematic Sunyaev–Zeldovich effect (e.g., Sunyaev & Zeldovich 1980; Dolag et al. 2005; Kashlinsky et al. 2008; Hand et al. 2012; Dolag et al. 2016; Planck Collaboration et al. 2016, 2020). However, due to signal weakness, it is a very difficult measurement. Therefore, ensemble statistics of peculiar velocities are more practical for current studies (e.g., Kaiser 1988; Ferreira et al. 1999; Juszkiewicz et al. 2000; Feldman et al. 2003; Watkins & Feldman 2007; Watkins et al. 2009; Feldman et al. 2010; Davis et al. 2011; Abate & Feldman 2012; Agarwal et al. 2012; Hand et al. 2012; Hellwing 2014; Nusser 2014; Kumar et al. 2015; Hoffman et al. 2016; Nusser 2016; Planck Collaboration et al. 2016; Scrimgeour et al. 2016, 2016; Seiler & Parkinson 2016; Hellwing et al. 2017).

Velocity correlation function analysis provides another tool to investigate the peculiar velocity field. The most widely used velocity correlation estimator was introduced by Gorski (1988) and further formulated by Gorski et al. (1989). It has provided interesting results constraining cosmological parameters (e.g., Jaffe & Kaiser 1995; Zaroubi et al. 1997; Borgani et al. 2000; Juszkiewicz et al. 2000; Abate & Erdoğdu 2009; Nusser & Davis 2011; Okumura et al. 2014; Hellwing et al. 2017; Howlett et al. 2017; Wang et al. 2018; Dupuy et al. 2019).

The velocity correlation function can be expressed as two independent functions, one for velocity components along the separation vector of a pair of galaxies and one for components perpendicular to this vector. The Gorski (1988) correlation estimator results in a complicated combination of these two functions, with the precise mixture given by selection functions that depend on the distribution of the survey objects as well as on the separation distance. This estimator has the decided disadvantage of not being comparable between studies that use different survey objects. Furthermore, at the time that it was introduced it was seen as being more stable than other methods given the small size of the available data sets. Given the availability of much larger peculiar velocity catalogs today, it is an opportune time to explore other methods of estimating velocity correlations. In addition, Wang et al. (2018) found that the cosmic variance of the correlation function using the Gorski estimator is large and non-Gaussian-distributed, and Hellwing et al. (2017) showed that it is susceptible to biases due to our special location near a large overdensity—the Virgo Cluster. These problems make the Gorski (1988) peculiar velocity correlation estimator less than ideal as a probe of the large-scale structure.

In this paper, we use an alternative method, introduced by Kaiser (1989) and Groth et al. (1989), that estimates the parallel and perpendicular correlation functions directly in a way that is independent of the survey distribution. This method further allows for the weighting of individual velocity measurements to account for the uneven sampling of the volume by peculiar velocity surveys. This is caused by two effects. First, the density of observed galaxies in a survey typically decreases with distance, so that the inner portions of the survey volume are more densely sampled than the outer portions. Second, peculiar velocity measurement uncertainties grow rapidly with distance, so that the measured velocities of nearby objects are much more accurate than those at greater distance. Both of these effects result in nearby galaxies carrying an outsized weight in most velocity analyses, leading to results that predominantly reflect the velocity field in a much smaller effective volume than expected from the scale of the survey. While Groth et al. (1989) used weighting to reduce the effect of random errors, we introduce a novel weighting scheme that reduces cosmic variance and bias by increasing the effective volume probed by a survey.

The paper is organized as follows: In Section 2, we derive the weighted estimators for the parallel and perpendicular correlation functions. In Section 3, we discuss the Cosmicflows-3 (CF3) catalog we analyze. In Section 4, we introduce the *N*-body simulations and methods used for generating mock catalogs. In Section 5, we show results for our method on both randomly centered mock catalogs and those centered in environments similar to that of the Milky Way for several different weighting schemes. We also apply our methods to obtain estimates of the parallel and perpendicular correlation functions in the local universe using data from the CF3 catalog. In Section 6, we discuss the parameter-constraining result using the weighted estimators. Section 7 concludes this paper.

2. The Peculiar Velocity Correlation Estimator

The general form of the two-point velocity correlation tensor is

$$\Psi_{ij}(\boldsymbol{r}) = \langle v_i(\boldsymbol{r_0}) v_j(\boldsymbol{r_0} + \boldsymbol{r})\rangle, \tag{1}$$

where i and j designate the Cartesian components of the velocity and the average is over points separated by the vector $\boldsymbol{r}$. Making the usual assumption that the velocity field is a statistically isotropic and homogeneous random field, we can write the correlation tensor in terms of two functions that depend only on the magnitude of the separation vector $r = |\boldsymbol{r}|$,

$$\Psi_{ij}(r) = \Psi_{\parallel}(r)\hat{r}_i\hat{r}_j + \Psi_{\perp}(r)(\delta_{ij} - \hat{r}_i\hat{r}_j) \tag{2}$$

where $\hat{r}$ is a unit vector in the direction of the separation vector. These two functions have simple physical interpretations: $\Psi_{\parallel}(r)$ is the (parallel) correlation of the velocity components along the separation vector and $\Psi_{\perp}(r)$ gives the (perpendicular) correlation of the components of the velocity perpendicular to the separation vector.

Our goal is to estimate $\Psi_{\parallel}(r)$ and $\Psi_{\perp}(r)$ from the correlations in the radial component of the peculiar velocity, u, which is the only component that can be measured. Given a pair of galaxies at positions $\boldsymbol{r}_1$ and $\boldsymbol{r}_2$, we can write the correlation of their radial peculiar velocities as

$$\begin{aligned}\langle u_1 u_2\rangle &= \hat{r}_{1i}\hat{r}_{2j}\langle v_i v_j\rangle \\ &= \Psi_{\parallel}(r)(\hat{\boldsymbol{r}}_1\cdot\hat{\boldsymbol{r}})(\hat{\boldsymbol{r}}_2\cdot\hat{\boldsymbol{r}}) \\ &+ \Psi_{\perp}(r)[\hat{\boldsymbol{r}}_1\cdot\hat{\boldsymbol{r}}_2 - (\hat{\boldsymbol{r}}_1\cdot\hat{\boldsymbol{r}})(\hat{\boldsymbol{r}}_2\cdot\hat{\boldsymbol{r}})].\end{aligned} \tag{3}$$

This expression can be written in terms of θ_1 and θ_2, the angles the separation vector $\boldsymbol{r}$ makes with the position vectors $\boldsymbol{r}_1$ and $\boldsymbol{r}_2$, respectively. Specifically,

$$(\hat{\boldsymbol{r}}_1\cdot\hat{\boldsymbol{r}})(\hat{\boldsymbol{r}}_2\cdot\hat{\boldsymbol{r}}) = \cos(\theta_1)\cos(\theta_2), \tag{4}$$

and

$$\begin{aligned}\hat{\boldsymbol{r}}_1\cdot\hat{\boldsymbol{r}}_2 &= \cos(\theta_2 - \theta_1) \\ &= \cos(\theta_1)\cos(\theta_2 + \sin(\theta_1)\sin(\theta_2).\end{aligned} \tag{5}$$

Using these results, we can put Equation (3) into the simple form

$$\langle u_1 u_2\rangle = \Psi_{\parallel}(r) f(\theta_1, \theta_2) + \Psi_{\perp}(r) g(\theta_1, \theta_2), \tag{6}$$

where $f = \cos(\theta_1)\cos(\theta_2)$ and $g = \sin(\theta_1)\sin(\theta_2)$.

Following Kaiser (1989) and Groth et al. (1989), we use a weighted least-squares method to estimate $\Psi_{\parallel}(r)$ and $\Psi_{\perp}(r)$ from a catalog of peculiar velocities u_m. We minimize the function

$$\begin{aligned}\chi^2(r) = \sum_{m,n} w_{m,n}[&u_m u_n \\ &- \Psi_{\parallel}(r) f(\theta_1, \theta_2) - \Psi_{\perp}(r) g(\theta_1, \theta_2)]\end{aligned} \tag{7}$$

with respect to $\Psi_{\parallel}(r)$ and $\Psi_{\perp}(r)$, where the sum is over pairs of galaxies whose separations fall within a specified bin and $w_{i,j}$ is a weight assigned to each galaxy pair. The minimization can be done analytically, resulting in the estimates

$$\Psi_{\parallel}(r) = \frac{\sum wg^2 \sum wfu_1u_2 - \sum wfg \sum wgu_1u_2}{\sum wf^2 \sum wg^2 - (\sum wfg)^2}, \tag{8}$$

and

$$\Psi_{\perp}(r) = \frac{\sum wf^2 \sum wgu_1u_2 - \sum wfg \sum wfu_1u_2}{\sum wf^2 \sum wg^2 - (\sum wfg)^2}, \tag{9}$$

where the sums are over galaxy pairs whose separations lie in a bin centered on r.

An alternative approach to studying peculiar velocity correlations is to use the ψ_1 and ψ_2 statistics introduced by Gorski et al. (1989) and utilized in several subsequent studies (e.g., Borgani et al. 2000; Hellwing et al. 2017; Wang et al. 2018). While these statistics in principle carry the same information as $\Psi_{\parallel}$ and $\Psi_{\perp}$, in practice they depend on the particular distribution of objects in a survey, making them not comparable between surveys. While in the past there was some motivation to focus on ψ_1 as being particularly stable when applied to the small data sets available at the time, there is now sufficient data to estimate $\Psi_{\parallel}$ and $\Psi_{\perp}$ directly. It is possible to calculate $\Psi_{\parallel}$ and $\Psi_{\perp}$ from ψ_1 and ψ_2 given the positions of the survey objects (see, e.g., Wang et al. 2018); however, this process can be shown to be mathematically equivalent to the calculations shown in Equations (8) and (9).

It is not obvious how to best choose weights to use in Equations (7), (8), and (9). Kaiser (1989) used the simplest choice, $w = 1$, while Groth et al. (1989) chose weights with an eye toward reducing the effects of measurement errors. However, previous work (Wang et al. 2018) has shown that, for the surveys we are working with, statistical errors are small

compared to the effects of cosmic variance, since we estimate the correlation function in a volume that is smaller than the scale of homogeneity. In general, the number density of galaxies nearby is higher than the number density of galaxies in the distant volume; this problem is exacerbated by the large measurement uncertainty of distant galaxies. This concentration of galaxies at small distances puts greater emphasis on the nearby volume, so that the effective volume reflected in the correlation functions can be significantly smaller than that of the survey. This effect increases the cosmic variance and may also lead to bias. Here we will weight the pairs in order to better balance the survey, so that it has a larger effective volume and hence smaller cosmic variance and bias but may lead to larger statistical errors.

Our approach will be to weight pairs of galaxies by the factor $w = (r_1 r_2)^p$, where r_1 and r_2 are the distances to the galaxies and p is a positive power. This scheme gives less weight to pairs of nearby galaxies, which are overrepresented in the sample, and greater weight to pairs of more distant galaxies, which are underrepresented. Correlation functions calculated using this weighting should thus sample the volume of the survey more evenly, and hence reflect a larger effective volume. However, in giving greater weight to galaxies that are far away, and hence have larger peculiar velocity uncertainties, our weighting scheme will necessarily increase statistical errors. We will explore several different choices for the power p in order to determine which value provides the best overall statistic for the data we are working with.

When analyzing data from simulations, we have access to all three components of the peculiar velocity. In this case we can calculate $\Psi_\parallel$ and $\Psi_\perp$ directly by taking a weighted average of the products of velocity components parallel and perpendicular to the separation vector for each pair, namely

$$\Psi_\parallel^{3D}(r) = \sum_{\text{pairs}} w(\boldsymbol{v_1}\cdot\boldsymbol{r})(\boldsymbol{v_2}\cdot\boldsymbol{r}) \Big/ \sum_{\text{pairs}} w \tag{10}$$

and

$$\Psi_\perp^{3D} = \frac{1}{2}\sum_{\text{pairs}} w[(\boldsymbol{v_1}\cdot\boldsymbol{v_2}) - (\boldsymbol{v_1}\cdot\boldsymbol{r})(\boldsymbol{v_2}\cdot\boldsymbol{r})] \Big/ \sum_{\text{pairs}} w, \tag{11}$$

where $\boldsymbol{r} = \boldsymbol{r_2} - \boldsymbol{r_1}$.

In linear theory, $\Psi_\parallel$ and $\Psi_\perp$ can be related directly to the power spectrum of density fluctuations $P(k)$ (Eisenstein & Hu 1998) through the relations

$$\Psi_\parallel(r) = \frac{(\sigma_8 f H_0)^2}{2\pi^2\sigma^2(8)}\int P(k)\left[j_0(kr) - 2\frac{j_1(kr)}{kr}\right]dk, \tag{12}$$

$$\Psi_\perp(r) = \frac{(\sigma_8 f H_0)^2}{2\pi^2\sigma^2(8)}\int P(k)\frac{j_1(kr)}{kr}dk, \tag{13}$$

where $f = \Omega_m^{0.55}$ (Linder 2005), H_0 is the Hubble constant, $j_n(x)$ denotes the spherical Bessel functions, and σ_8 is the amplitude of density fluctuations on a scale of 8 h^{-1} Mpc. In the equations, σ_8 is the value from the simulation we use (see Section 4) and $\sigma(8)$ is calculated following the method in Eisenstein & Hu (1998, Equation A7).

3. Data

The CF3 peculiar velocity compilation (Tully et al. 2016) includes two catalogs: the galaxy catalog and the group catalog. The CF3 galaxy catalog contains 17,669 galaxies, including all the 8135 galaxy distances in Cosmicflows-2 (Tully et al. 2013), which is a compilation of Type Ia supernovae (Tonry et al. 2003), Tully–Fisher (TF) spiral galaxy clusters (Giovanelli et al. 1998; Dale et al. 1999), Streaming Motions of Abell Clusters (SMAC) from FP survey (Hudson et al. 1999, 2004), FP early-type far galaxy clusters (Colless et al. 2001), TF clusters (Willick 1999), the SFI++ catalog (Masters et al. 2006; Springob et al. 2007, 2009), the SFI++ group catalog (Springob et al. 2009), an early-type nearby galaxy survey (da Costa et al. 2000; Bernardi et al. 2002; Wegner et al. 2003), and a surface brightness fluctuation survey (Tonry et al. 2001), together with 2257 distances derived from the correlation between galaxy rotation and luminosity with photometry at 3.6 μm obtained with the Spitzer Space Telescope and 8885 distances based on the FP sample derived from the Six-degree Field Galaxy Survey (Springob et al. 2014). The CF3 group catalog contains 11,878 groups and galaxies, where galaxies in known groups have had their distance moduli and redshifts averaged, resulting in a single velocity and position for the group as a whole. Due to this averaging, the peculiar velocities of the groups have reduced uncertainties as compared to the individual galaxies. However, Dupuy et al. (2019) suggest that using grouped data to constrain the growth rate might lead to incoherent results. In the following analyses, we will use the CF3 galaxy catalog.

The peculiar velocities of CF3 are calculated through the unbiased peculiar velocity estimator introduced by Watkins & Feldman (2015):

$$v = cz\log\left(\frac{cz}{H_0 r}\right). \tag{14}$$

The redshift (cz) and distance (r) are provided by the CF3 survey; however, the choice of the value of the Hubble constant will affect the peculiar velocity and therefore the velocity correlation result. Wang et al. (2018) discussed the effect of the Hubble constant on the Gorski (1988) correlation functions. For this study we will set the Hubble constant equal to 75 km s^{-1} Mpc^{-1} for the peculiar velocities of the CF3 survey; Tully et al. (2016) have shown that this is the value that minimizes the magnitude of radial flows.

Due to large uncertainties in distance measurements, previous studies of the velocity correlation functions (e.g., Gorski 1988; Borgani et al. 2000; Wang et al. 2018) have used redshifts to determine the positions of objects and hence the separations between them. Distances given by cz/H_o differ from the actual distances by an "error" of the peculiar velocity divided by the Hubble constant, which can be much smaller than the measurement uncertainty for measured distances. In Wang et al. (2018) we found that using the estimated distances to estimate the galaxy pair separation leads to unreliable ψ_1 and ψ_2 results. Considering the relations among ψ_1, ψ_2, $\Psi_\parallel$, and $\Psi_\perp$, redshift is also the optimal choice for the $\Psi_\parallel$ and $\Psi_\perp$ separations. Therefore, even though using redshift as the separation may lead to redshift distortion effects, it is still more reliable than distance estimation, whose large uncertainty causes biases. In this paper we will also use redshifts to determine the positions of the objects in our catalog, using distance estimates only in our calculation of peculiar velocities.

4. Mock Catalogs

The mock catalogs we use in this paper were generated from the halo catalogs of the Outer Rim Simulation (Habib et al. 2016; Heitmann et al. 2019a, 2019b), which was carried out

Table 1
The Cosmological Parameters of the Outer Rim Simulation

Matter density, Ω_m	0.2648
Cosmological constant density, Ω_Λ	0.7352
Baryon density, Ω_b	0.0448
Hubble parameter, h (100 km s^{-1} Mpc^{-1})	0.71
Amplitude of matter density fluctuations, σ_8	0.8
Primordial scalar spectral index, n_s	0.963
Box size (h^{-1} Gpc)	3.0
Number of particles	$10,240^3$
Particle mass, m_p (10^9 h^{-1} $M_\odot$)	1.85
Softening, f_c (h^{-1} kpc)	3

from the Mira-Titan Universe Simulations. The Outer Rim Simulation is a dark-matter-only simulation with cosmological parameters similar to the Wilkinson Microwave Anisotropy Probe 7 (Larson et al. 2011) cosmology, which are shown in Table 1.

The simulation contains halos with a large range of masses that covers galaxies, groups, and clusters. We used halos in the mass range $[10^{11}, 10^{13}]$ $M_\odot$ located in the inner $(1.5\ h^{-1}\ \mathrm{Gpc})^3$ volume of the Outer Rim Simulation box as galaxies to generate mock catalogs that mimic the CF3 galaxy survey. Figure 1 shows the redshift distribution of the CF3 galaxy catalog and an example of the mock catalogs.

We found that choosing mock catalog galaxies to match the CF3 selection function based on redshifts or distances has no significant impact on the correlation function. As discussed above, we chose the redshift selection function in generating mock catalogs since, given the large uncertainty in distance estimates, redshift provides a more accurate distance.

We generated two kinds of mock catalogs for the error analysis of the correlation function: catalogs for cosmic variance and catalogs for statistical errors. The cosmic variance mocks (M_c^i) are centered at randomly distributed positions without any peculiar velocity measurement uncertainties, where M_c^i represents the cosmic variance mock located at the ith center. The cosmic variance was calculated by taking the standard deviations of the velocity correlation functions of the cosmic variance mocks ($\sigma_c = \mathrm{STD}\{M_c^1, M_c^2, \cdots, M_c^{100}\}$). We used two types of cosmic variance mock catalogs differing in how their halo center points were chosen. The first type, which we call random mocks, is centered on randomly chosen halos inside the inner $(1.5\ h^{-1}\ \mathrm{Gpc})^3$ region of the simulation. The second type, called Local Group (LG) mocks, is centered on a Milky Way–like halo ($M = [13.5 \pm 6.5] \times 10^{11}\ h^{-1} M_\odot$) with a Virgo-like cluster at a distance similar to that of the Virgo Cluster from the Milky Way. The LG selection criterion is based on that introduced by Hellwing et al. (2017). These catalogs are useful for exploring the observational consequences of our nontypical location in the universe, a region whose dominant characteristic is the neighboring Virgo-like cluster ($M = [1.2 \pm 0.6] \times 10^{15}\ h^{-1} M_\odot$) at a distance of $12 \pm 4\ h^{-1}$ Mpc.

For each type of observer, we generated 100 mock catalogs. With the mock catalog centers selected randomly, it would be hard to avoid overlapping between them. However, the overlapping is not significant in such a large volume. For the random observers, only 7.6% of the pairs of mock centers are closer than 300 h^{-1} Mpc to each other. For the LG observers, 7% of them are closer than 200 h^{-1} Mpc and 15% of them are closer than 300 h^{-1} Mpc. Considering the maximum depth of the CF3 galaxy survey is about 170 h^{-1} Mpc (Figure 1) and the galaxy separations of interest for this study are smaller than 100 h^{-1} Mpc, the overlapping is negligible.

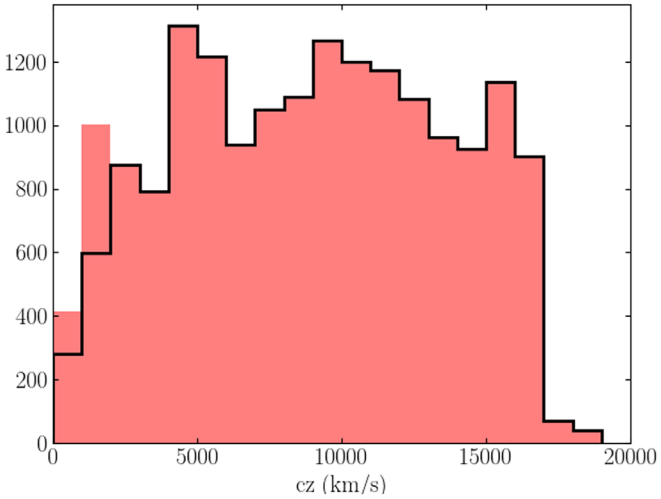

Figure 1. The redshift distribution of the full CF3 galaxy catalog (red histogram). The black-lined histogram shows an example of the mock catalogs.

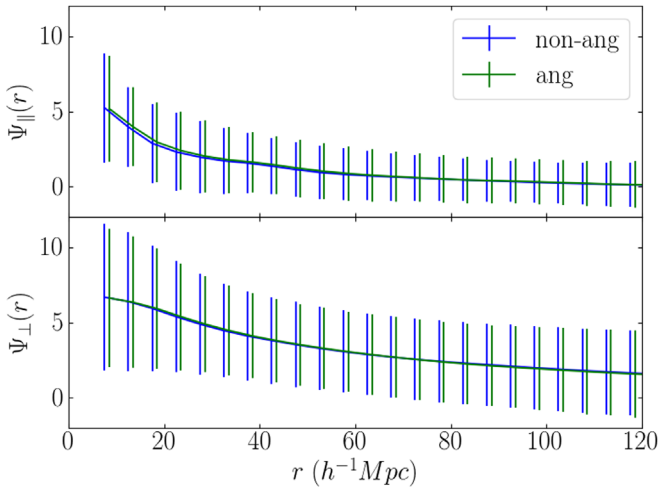

Figure 2. $\Psi_\parallel$ and $\Psi_\perp$ results of mock catalogs with (green) and without (blue) the anisotropy of the CF3 angular distribution. The error bars show the total error of the correlations.

We also generated mock catalogs that mimic the angular distribution of the CF3 objects, which is significantly anisotropic. However, we found that the anisotropy of the CF3 angular distribution does not have a significant effect on the correlation functions, as shown in Figure 2.

The statistical error mock catalogs ($M_{s_j}^i$) were generated by perturbing the distances (and hence the peculiar velocities) of the objects in a cosmic variance mock catalog with the average CF3 distance measurement uncertainty (20%), where $M_{s_j}^i$ represents the jth perturbed statistical error mock catalog at the ith center. The statistical error of the ith cosmic variance mock catalog was calculated by taking standard deviations over 100 versions of the statistical error mock catalogs ($\sigma_s^i = \mathrm{STD}\{M_{s_1}^i, M_{s_2}^i, \cdots, M_{s_{100}}^i\}$), while the statistical error of the velocity correlation function was calculated by taking the average of the statistical errors

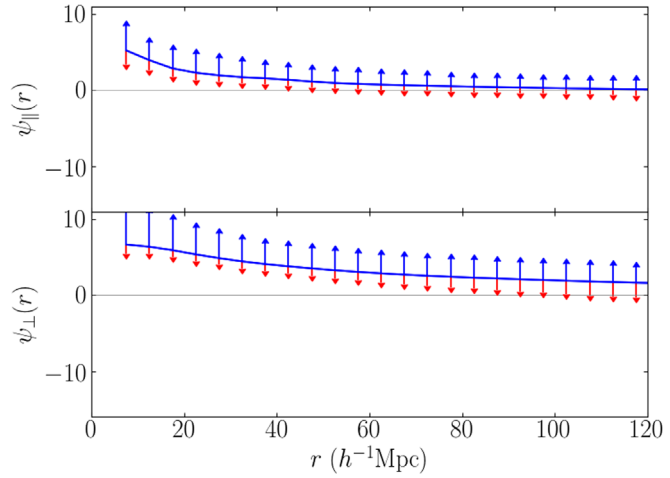

Figure 3. The parallel and perpendicular correlation functions of randomly centered mock catalogs with uniform weighting. $\Psi_\parallel$ and $\Psi_\perp$ are in units of (100 km s^{-1})^2. The blue solid lines show the average values for 100 mock catalogs. The upper blue error bars show the cosmic variance. The lower red error bars indicate the statistical error.

over 10 randomly selected cosmic variance mock catalogs ($\sigma_s = \mathrm{AVE}\{\sigma_s^i\}_{10}, i \in [1, 100]$).

5. Results

Figure 3 shows $\Psi_\parallel$ and $\Psi_\perp$ and their cosmic variance (upper) and statistical errors (lower) using randomly centered mock catalogs with uniform weighting. In the figure, the cosmic variance, which is larger than the statistical errors (especially for closer pairs), dominates the error budget. This is consistent with the Wang et al. (2018) results, which showed that the cosmic variance is the dominant source of error in the Gorski correlation functions, which use uniform weighting. Wang et al. (2018) also showed that the error distribution of the function ψ_1 is significantly non-Gaussian. Below we will examine the question of the distribution of the correlation functions in more detail.

Figure 4 shows the cosmic variance distribution of $\Psi_\parallel$ and $\Psi_\perp$ calculated from our estimators using uniform weighting, and ψ_1 and ψ_2 calculated using the Gorski (1988) formalism, for 100 randomly centered mock catalogs. We show the distributions for a particular bin (40–45 h^{-1} Mpc) as an example. In the figure, we see that $\Psi_\parallel$ and ψ_2 have roughly Gaussian distributions, while the distributions of $\Psi_\perp$ and ψ_1 are noticeably skewed, with significant non-Gaussian tails; these distributions generally become more non-Gaussian in larger-separation bins. The similarity between $\Psi_\parallel$ and ψ_2 is not surprising, since ψ_2 was calculated from the projections of the radial velocities onto the separation vectors. The other Gorski correlation function, ψ_1, was estimated from the unprojected radial velocity, making it a combination of $\Psi_\parallel$ and $\Psi_\perp$. The cosmic variance of $\Psi_\parallel$ is roughly Gaussian except for scales smaller than 10 h^{-1} Mpc, where the uncertainty of the correlation function is large. Considering the large uncertainty and possibly non-Gaussian cosmic variance in small-separation bins, we recommend that small-scale correlations ($\lesssim 10\,h^{-1}$ Mpc) not be used in parameter constraints. Quantities with non-Gaussian distributions are difficult to interpret, suggesting that studies of the velocity correlation function should focus on $\Psi_\parallel$. We will return to this issue in Section 7.

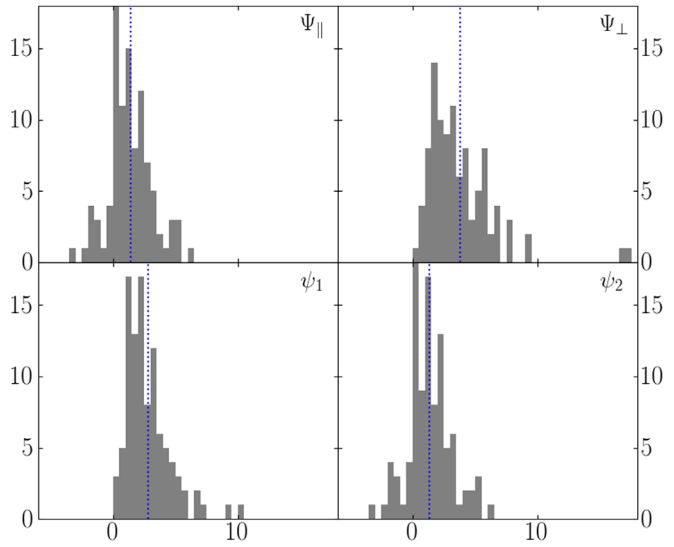

Figure 4. The distribution of $\Psi_\parallel$, $\Psi_\perp$, ψ_1, and ψ_2 in 40–45 h^{-1} Mpc bins of 100 randomly centered mock catalogs using uniform weighting, in units of (100 km s^{-1})^2. The vertical blue dotted line is the mean of the mock catalogs.

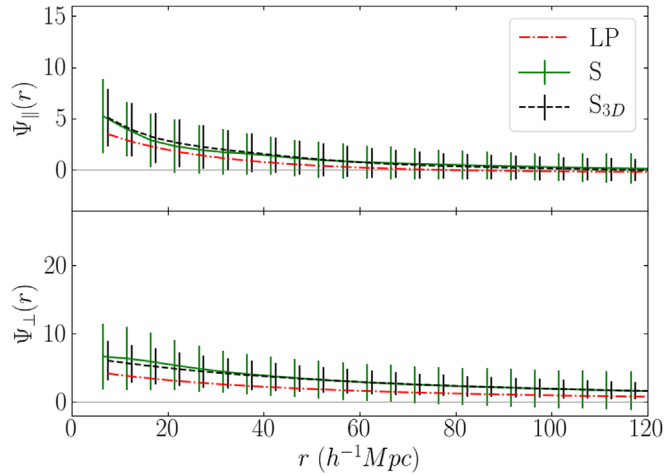

Figure 5. The parallel and perpendicular correlation functions of 100 randomly centered mock catalogs in units of (100 km s^{-1})^2. The red dashed–dotted lines show the linear predictions (LP). The green solid lines indicate the average of the mock catalog results calculated using the estimators discussed in the text (S). The black dashed lines indicate the average of the mock catalog results for the full 3D velocity fields (S_{3D}). The error bars show the cosmic variance of the mock catalogs.

Figure 5 shows the $\Psi_\parallel$ and $\Psi_\perp$ estimators (Equations (8) and (9)) and 3D velocity fields (Equations (10) and (11)) calculated using randomly centered mock catalogs. The simulation results agree well with linear predictions for both $\Psi_\parallel$ and $\Psi_\perp$. Although the estimators use only line-of-sight peculiar velocities, they also agree well with the full 3D results, lending credence to their efficacy and stability. It should be noted again that there is the potential of redshift distortion effects between the mock catalog results and the linear theory prediction, since the correlation function was calculated with redshift separations while the linear prediction was calculated from distance separations. However, our results indicate that these effects are not significant.

Hellwing et al. (2017) discussed the effect of observer location on velocity statistics. They compared both the Gorski

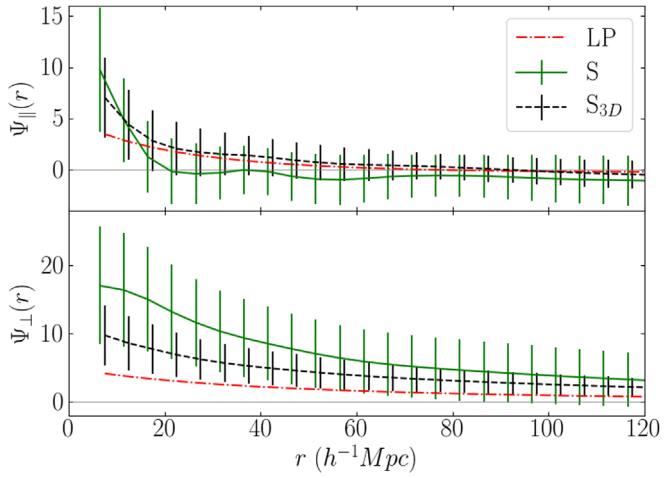

Figure 6. Same as Figure 5 but using LG-centered mock catalogs.

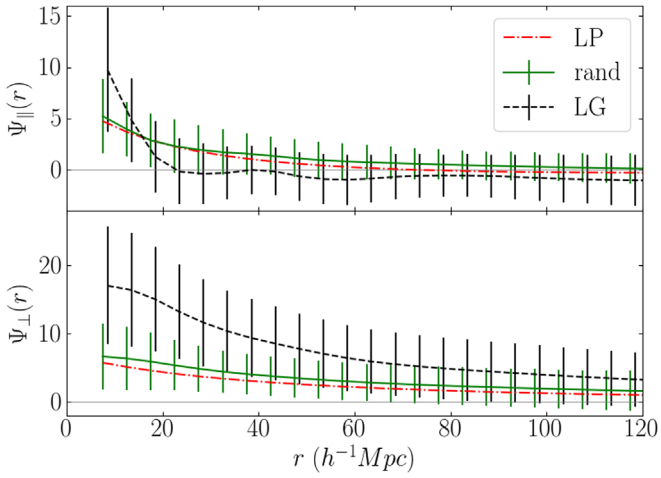

Figure 7. Parallel and perpendicular correlation results of 100 randomly centered and 100 LG-centered mocks in units of (100 km s^{-1})^2 using uniform weighting ($w = 1$). All mock catalogs have had galaxy distances perturbed by random measurement errors. The red dashed–dotted lines show the linear predictions. The green solid lines indicate the average results for the randomly centered mocks. The black dashed lines show the average results for the LG-centered mocks. The error bars show the total error of the correlation function, which includes both cosmic variance and statistical error.

velocity correlation function estimators and the pairwise velocity statistic calculated for mock catalogs with random halo centers and for those centered on locations that mimicked the LG. They found that the correlation functions calculated from the LG-like catalogs exhibited significant bias relative to linear theory. To study the effects of observer location on the parallel and perpendicular correlation functions, in Figure 6 we show the results of using LG-centered mock catalogs. We see that $\Psi_{\parallel}$ and $\Psi_{\perp}$ for the LG-centered mocks with uniform weighting are also biased. As we discuss below, this bias can be greatly reduced through the use of weighting.

Figure 6 shows the parallel and perpendicular correlation results of using LG-centered mock catalogs with uniform weighting ($w = 1$). We see that the restriction to LG-like locations introduces significant systematic bias into our results relative to linear theory. This bias takes two distinct forms. First, we see that both our estimators, which use only radial velocities, do not accurately recover the 3D correlation function. Second, we see that, especially for the perpendicular correlation function, the average correlations calculated from the 3D velocities also do not accurately reflect linear theory. Both of these biases arise most likely because the volumes around the LG-centered mocks are not typical, but rather exhibit particular flow patterns that are significantly different from the averages taken over random volumes.

Figure 7 shows a comparison between random and LG-centered mocks. The error bars of the simulation results show the total error ($\sigma_t = \sqrt{\sigma_c^2 + \sigma_s^2}$, where σ_t is the total error, σ_c is the cosmic variance, and σ_s is the statistical error) of the correlation functions. We see that the variance of the LG-centered mock catalogs is significantly larger than that of the randomly centered mock catalogs, particularly for the perpendicular correlation function ($\Psi_{\perp}$).

The fact that the bias in the estimated correlation functions with uniform weights in LG-centered mocks has the same order of magnitude as the correlation functions themselves suggests that correlation functions calculated using CF3 with uniform weights, which include those calculated using the Gorski method, should not be used in comparisons with linear theory.

As discussed above, weighting can be used to increase the effective volume of the survey. Our approach will be to weight galaxy pairs by $w = (r_1 r_2)^p$, where r_1 and r_2 are the distances of the two galaxies and p is a non-negative power. In the LG-centered mocks, this weighting reduces emphasis on the relatively small volume near the center of the survey, which for the LG-centered mocks is atypical. We will see that the use of weighting can effectively reduce the bias found in the LG-centered mocks.

Figure 8 shows the results based on weights $w = (r_1 r_2)^p$ with $p = 0.5$, 1, and 2 ($p = 0$ gives uniform weights). The use of weighting has reduced the bias to an insignificant level. However, the total error becomes larger while the effective volume of the surveys increases.

Figure 9 shows the cosmic variance and the statistical errors of the weighted correlation functions with $p = 0.5$ ($w = (r_1 r_2)^{1/2}$), $p = 1$ ($w = r_1 r_2$), and $p = 2$ ($w = (r_1 r_2)^2$). The cosmic variance generally decreases with weighting as expected; however, the statistical errors increase and dominate when using weights with larger p. In addition, both our result and the result from Hellwing et al. (2017) show that the cosmic variance of LG observers is larger than that of random observers. Hellwing et al.'s (2017) explanation is that different observers see different radial velocity components for the same galaxies.

Considering the decreasing trend of the cosmic variance with the weight power, we suggest that the large cosmic variance of LG observers may also be caused by an imbalanced (nearby-galaxy-dominated) distribution of galaxies. When the galaxy distribution is imbalanced, the galaxy distribution around a big attractor (e.g., the Virgo Cluster) may lead to various biases and large cosmic variance. Table 2 shows the cosmic variance and statistical errors of $\Psi_{\parallel}$ with different weighting schemes; even as cosmic variance decreases, we see the total error increase. Considering the trade-offs, $p = 1$ ($w = r_1 r_2$) seems to be the best value to use for the CF3 survey. However, the optimal value of p may vary for different surveys due to the specific object distributions and uncertainties.

Now that we have determined that $p = 1$ provides the optimal weighting for our analysis, we apply our methods to the actual CF3 galaxy catalog. In Figure 10, we show the parallel and perpendicular correlation functions for the CF3 galaxy catalog, using the $p = 1$ ($w = r_1 r_2$) weighting scheme, together with the results (with the estimated total uncertainties, including the cosmic

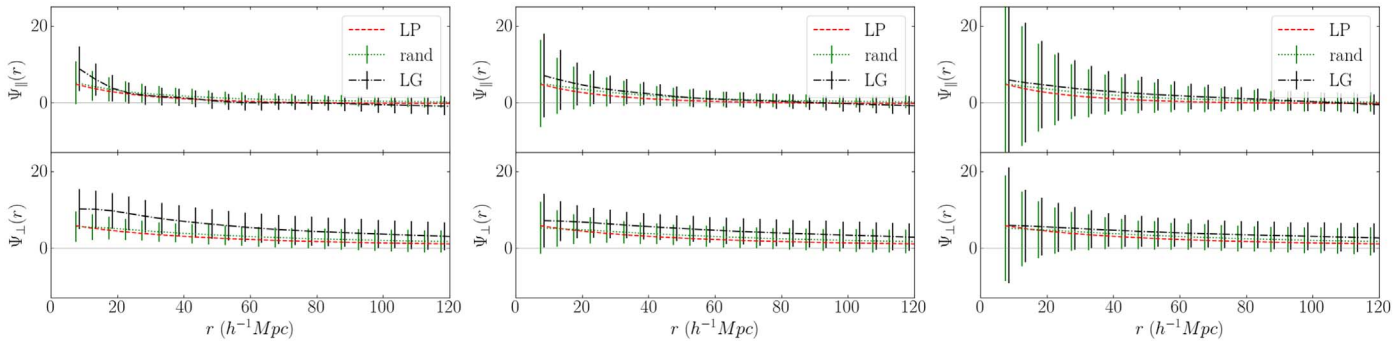

Figure 8. Same as Figure 7 but using the position-weighted method with weights $p = 0.5$ (left panel), $p = 1$ (middle panel), and $p = 2$ (right panel).

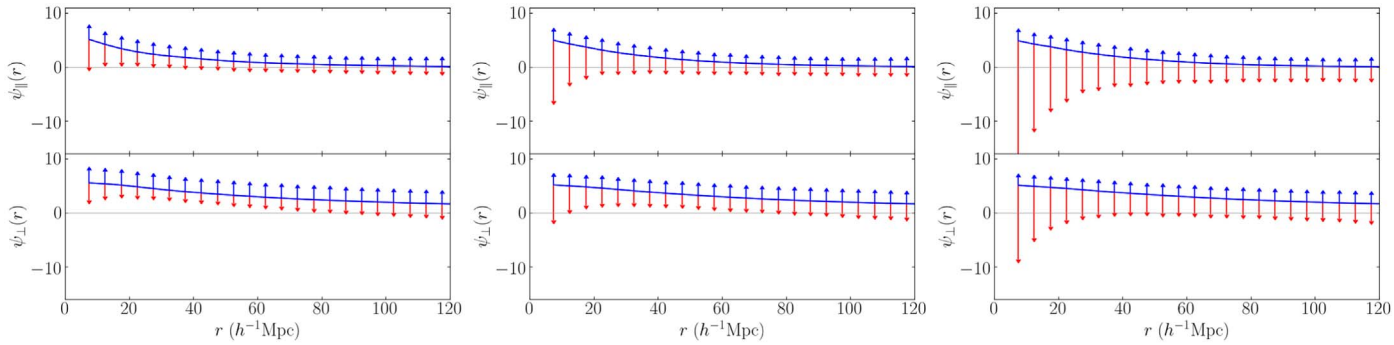

Figure 9. The parallel and perpendicular correlation functions with weights $p = 0.5$ (left panel), $p = 1$ (middle panel), and $p = 2$ (right panel). $\Psi_\parallel$ and $\Psi_\perp$ are in units of (100 km s^{-1})^2. The blue solid lines show averages over 100 mock catalogs. The upper blue error bars show the cosmic variance. The lower red error bars indicate the statistical errors.

Table 2
The Errors of $\Psi_\parallel$ with Random Observers Using Various Weighting Schemes

Weight	p		(15–20)	(35–40)	(55–60)
1	0	σ_c	2.45	1.88	1.59
		σ_s	0.95	0.66	0.66
		σ_t	2.63	1.99	1.72
$\sqrt{r_1 r_2}$	0.5	σ_c	1.78	1.48	1.29
		σ_s	2.58	1.45	1.13
		σ_t	3.13	2.07	1.71
$r_1 r_2$	1	σ_c	1.59	1.37	1.14
		σ_s	5.37	2.54	1.79
		σ_t	5.6	2.89	2.12
$(r_1 r_2)^2$	2	σ_c	1.59	1.47	1.27
		σ_s	11.39	5.04	3.36
		σ_t	11.5	5.25	3.59

Note. The σ_t, σ_c, and σ_s indicate the total error, cosmic variance, and statistical error of the correlation function in units of (100 km s^{-1})^2, respectively. The numbers in brackets show the separation range of the three selected bins (in units of h^{-1} Mpc).

variance and measurement errors) of both the randomly centered and LG-centered mock catalogs with the same weighting. We see that both $\Psi_\parallel$ and $\Psi_\perp$ have the expected behavior: decreasing amplitude with increasing separation. Also as expected from linear theory, $\Psi_\perp$ decreases more slowly and has larger amplitude than $\Psi_\parallel$ at large separation. Considering the magnitudes of the total uncertainties, both $\Psi_\parallel$ and $\Psi_\perp$ are consistent (within two standard deviations) with the results from the mock catalogs, and thus consistent with the standard cosmological model.

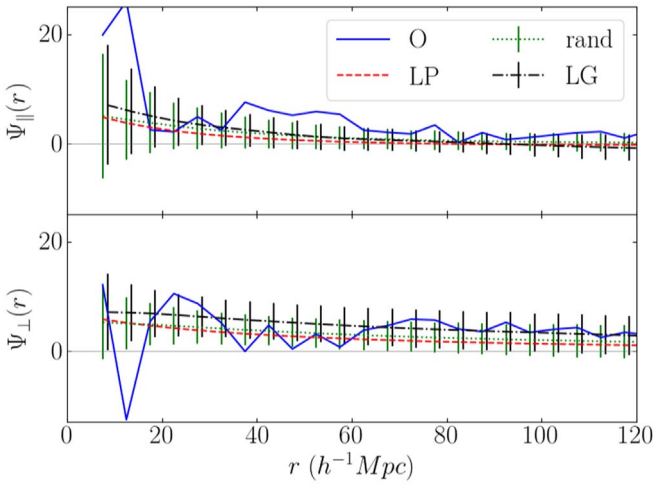

Figure 10. The blue dotted lines indicate the parallel and perpendicular correlation estimates in units of (100 km s^{-1})^2 calculated from the CF3 galaxy catalog using the weighting scheme $w = r_1 r_2$ ($p = 1$). The red dashed–dotted lines show the linear prediction. The green solid lines indicate the average results from the randomly centered mock catalogs with the same weighting. The black dashed lines show the average results from the LG-centered mocks, also with the same weighting. The error bars show the total uncertainty, including the cosmic variance and measurement errors.

6. Parameter Constraints

In Wang et al. (2018), we showed that the correlation function ψ_1 has a long, non-Gaussian tail in its cosmic variance distribution, making it unsuitable for placing constraints on cosmological parameters. As we discussed in Section 5, the cosmic variance of $\psi_\parallel$ exhibits a better approximation of a

Gaussian distribution than ψ_1. This suggests that $\psi_\parallel$ may be a more useful measurement of peculiar velocity correlations. In this section, we test the performance of uniformly weighted and position-weighted $\psi_\parallel$ with both random and LG observers with respect to putting constraints on cosmological parameters.

As can be seen in Figure 9, the statistical errors increase with weighting even as the cosmic variance decreases. To gauge the effects of statistical errors and cosmic variance separately and together, we implemented three methods for cosmological parameter estimation. To look at the effects of cosmic variance alone, we used mock catalogs drawn from different regions of the simulation box with no measurement errors in their velocities (as described above) with the χ^2 given by

$$\chi^2_{\rm c} = \sum_{i,j} [\psi^C_\parallel(r_i) - \psi^{\rm L}_\parallel(r_i)]\, C^{-1}_{ij}\, [\psi^C_\parallel(r_j) - \psi^{\rm L}_\parallel(r_j)], \quad (15)$$

where

$$C_{ij} = \frac{1}{N_{\rm mock}} \sum_{l=1}^{N_{\rm mock}} (\Psi^i_{\parallel,l} - \overline{\Psi}^i_{\parallel,C})(\Psi^j_{\parallel,l} - \overline{\Psi}^j_{\parallel,C}). \quad (16)$$

$\chi^2_{\rm c}$ (Equation (15)) is the cosmic variance (C) covariance matrix, $N_{\rm mock} = 100$ is the number of mock catalogs, $\psi^i_{\parallel,l}$ is the correlation value of the ith separation bin of the lth mock catalog, $\overline{\psi}^i_{\parallel,C}$ is the average value of the $N_{\rm mock}$ catalogs in the ith separation bin, $\psi^C_\parallel$ is the average value of $\psi_\parallel$ over the $N_{\rm mock}$ mock catalogs, and $\psi^{\rm L}_\parallel$ is the linear prediction.

To look at the effects of measurement errors alone, we used 100 versions of one mock catalog perturbed with artificial measurement errors with the χ^2 function:

$$\chi^2_{\rm s} = \sum_{i,j} [\psi^{\rm S}_\parallel(r_i) - \psi^{\rm L}_\parallel(r_i)]\, \varepsilon^{-1}_{ij} \times [\psi^{\rm S}_\parallel(r_j) - \psi^{\rm L}_\parallel(r_j)], \quad (17)$$

where

$$\varepsilon_{ij} = \frac{1}{N_{\rm pert}} \sum_{p=1}^{N_{\rm pert}} (\Psi^i_{\parallel,p} - \Psi^i_{\parallel,A})(\Psi^j_{\parallel,p} - \Psi^j_{\parallel,A}). \quad (18)$$

$\chi^2_{\rm s}$ (Equation (17)) uses the covariance matrix that contains the information of statistical errors, where ε is the covariance matrix of statistical errors, $N_{\rm pert}$ is the number of perturbed catalogs of a selected mock catalog whose value is closest to the average value of the 100 mock catalogs, $\psi^i_{\parallel,A}$ is the parallel correlation of the selected mock catalog in the ith separation bin, $\psi^i_{\parallel,p}$ is the correlation value of the ith separation bin of the pth perturbed catalog of the selected mock catalog, and $\psi^{\rm S}_\parallel$ is the average value over the $N_{\rm pert}$ perturbed catalogs of the selected mock catalog.

Finally, to look at the effects of cosmic variance and statistical errors together, we used 100 mock catalogs drawn from different parts of the simulation box, each perturbed with measurement errors. The χ^2 for these catalogs is given by

$$\chi^2_{\rm t} = \sum_{i,j} [\psi^T_\parallel(r_i) - \psi^{\rm L}_\parallel(r_i)]\, T^{-1}_{ij}\, [\psi^T_\parallel(r_j) - \psi^{\rm L}_\parallel(r_j)], \quad (19)$$

where

$$T_{ij} = \frac{1}{N_{\rm mp}} \sum_{n=1}^{N_{\rm mp}} (\Psi^i_{\parallel,n} - \overline{\Psi}^i_{\parallel,T})(\Psi^j_{\parallel,n} - \overline{\Psi}^j_{\parallel,T}). \quad (20)$$

$\chi^2_{\rm t}$ (Equation (17)) includes the effect of both the cosmic variance and the statistical errors, where T is the covariance matrix of the total error; $N_{\rm mp}$ is the number of perturbed mock catalogs, which means perturbing each of the 100 mock catalogs one time randomly according to the distance uncertainties to get 100 perturbed mock catalogs; $\psi^i_{\parallel,n}$ is the correlation value of the ith separation bin of the nth perturbed mock catalog; $\overline{\psi}^i_{\parallel,T}$ is the average value of the $N_{\rm mp}$ perturbed mock catalogs in the ith separation bin; and $\psi^T_\parallel$ is the average value over the $N_{\rm mp}$ perturbed mock catalogs.

Figure 11 shows the cosmological parameter constraints for $\Omega_{\rm m}$ and σ_8 using $\Psi_\parallel$ in separation scales of [1000, 6000] km s^{-1} with bin widths equal to 500 km s^{-1}, which are used consistently in the following parameter constraints. In our tests, we find the results based on $\Psi_\parallel$ are much more stable than those based on ψ_1 for implementing different truncations (see also Wang et al. 2018).

For the $\chi^2_{\rm c}$ fitting method, all of the four correlation weights, $p = 0$ ($w = 1$), $p = 0.5$ ($w = (r_1 r_2)^{1/2}$), $p = 1$ ($w = r_1 r_2$), and $p = 2$ ($w = (r_1 r_2)^2$), agree with the simulation value within 1σ for both the random and LG observers. However, the results of the uniformly weighted $\Psi_\parallel$ with the LG observers are not as consistent as the results of the random observers. The position-weighted method improves the parameter constraints for the LG observers significantly, since the position weighting scheme reduces the bias. The position weighting scheme also provides tighter and more stable constraints than the uniformly weighted $\Psi_\parallel$. In addition, the position-weighted $\Psi_\parallel$ provides tighter constraints on the expected value (simulation value) for both the random and LG observers. Comparing the results of the three position-weighted $\Psi_\parallel$, we find $p = 1$ provides the best results.

In the $\chi^2_{\rm s}$ plots, the result of the uniformly weighted $\Psi_\parallel$ biases the simulation value for both the random and LG observers. However, the position-weighted correlation function agrees with the simulation value within 1σ for both types of observers, except $p = 2$ for the LG observers. Similar to the results of the $\chi^2_{\rm c}$ method, the uniformly weighted $\Psi_\parallel$ provides biased parameter constraints for the LG observers, which are greatly improved by the position weighting scheme. However, unlike that in $\chi^2_{\rm c}$, the position-weighted $\Psi_\parallel$ has laxer constraining contours than the uniformly weighted $\Psi_\parallel$. This is due to the larger statistical errors caused by the larger position weighting power.

To study the effect of the size of the statistical uncertainty on the $\chi^2_{\rm t}$ constraining method, we implemented different distance uncertainty percentages (distance uncertainties equal to 5%, 10%, 15%, and 20% of the distance) as shown in Figure 12. In the figure, the position-weighted correlations show significant improvements in the LG observers for all of the four uncertainty percentages. However, the $\chi^2_{\rm t}$ constraining contour becomes large when the distance perturbation is larger than 10%. Therefore a CF3-like survey with 20% distance errors will probably not be able to put meaningful constraints on the cosmological parameters.

Much larger peculiar velocity surveys should be available in the not-too-distant future. Having more survey objects will improve constraints in two main ways. First, since the correlation function is essentially an average, having more survey objects will reduce statistical errors in the usual way. However, having more survey objects, particularly at large distances, will also allow us to reduce cosmic variance by using a more aggressive weighting scheme and therefore increasing the effective volume that the survey probes. In other words, if

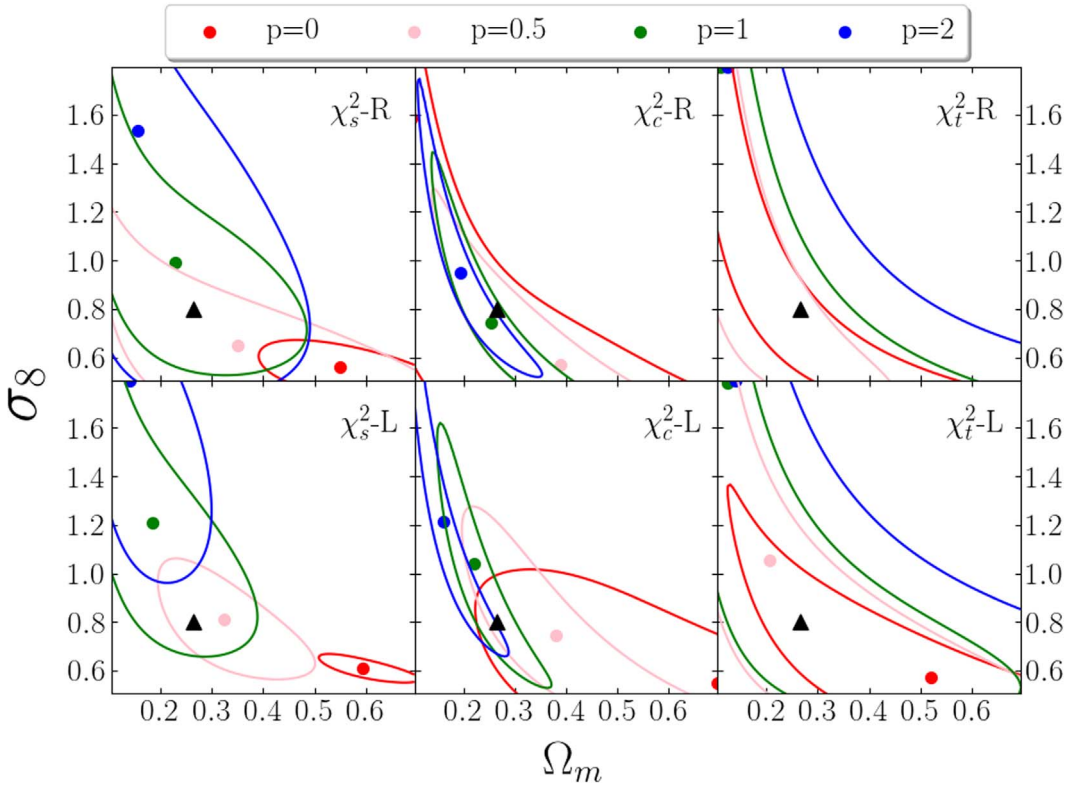

Figure 11. Ω_m and σ_8 constraints using simulation data with bins equal to 500 km s^{-1} within separation scales of [1000, 6000] km s^{-1}. The minimum χ^2 value has been subtracted from each cell. The contours indicate the 68% likelihood of the χ^2 values. The triangle marker indicates the value from the Outer Rim Simulation. χ_c^2 shows the result of the covariance matrix with cosmic variance, χ_s^2 indicates the result of the covariance matrix with statistical errors, and χ_t^2 includes the information of both the cosmic variance and the statistical errors. R and L indicate the random and LG observers, respectively.

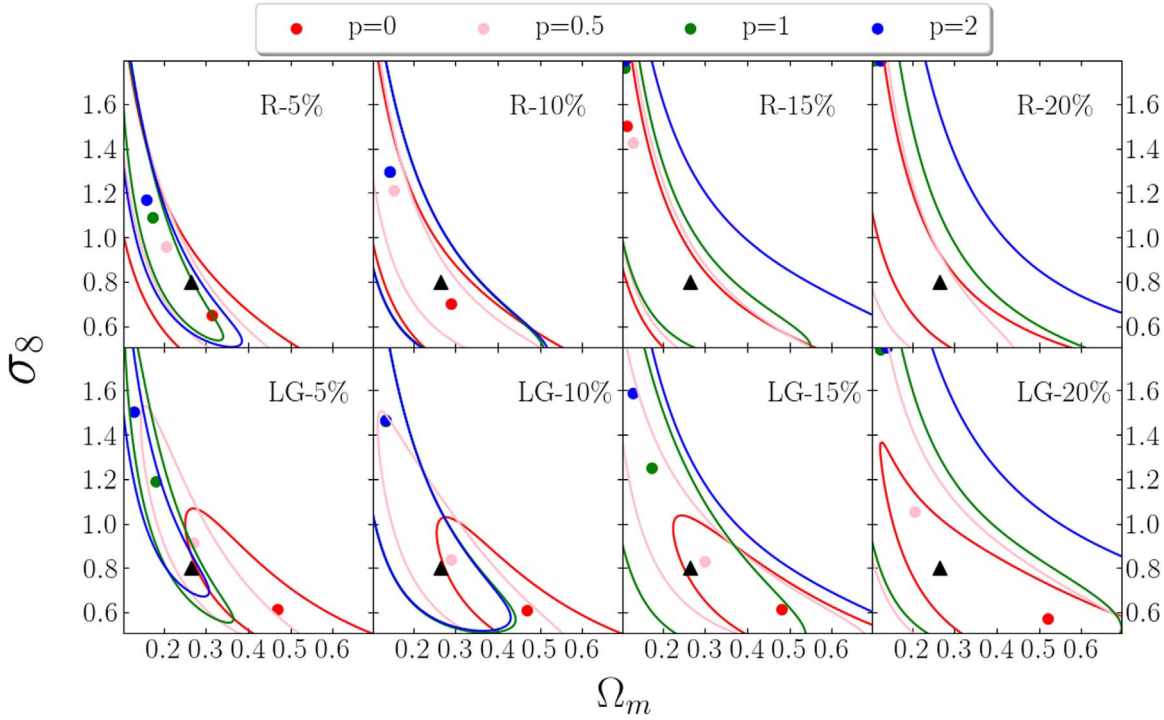

Figure 12. Ω_m and σ_8 constraints of χ_t^2 with different distance perturbation values. The minimum χ_t^2 value has been subtracted from each cell. The contours indicate the 68% likelihood values. The triangle marker indicates the value from the Outer Rim Simulation. R and LG indicate the random and LG observers, respectively.

the statistical errors start small, then we can afford to have them increase more in our effort to reduce cosmic variance. Without weighting, increasing the number of survey objects without substantially increasing survey depth will have less effect, since statistical errors are currently dominated by cosmic variance. As the size of peculiar velocity surveys increases, our method

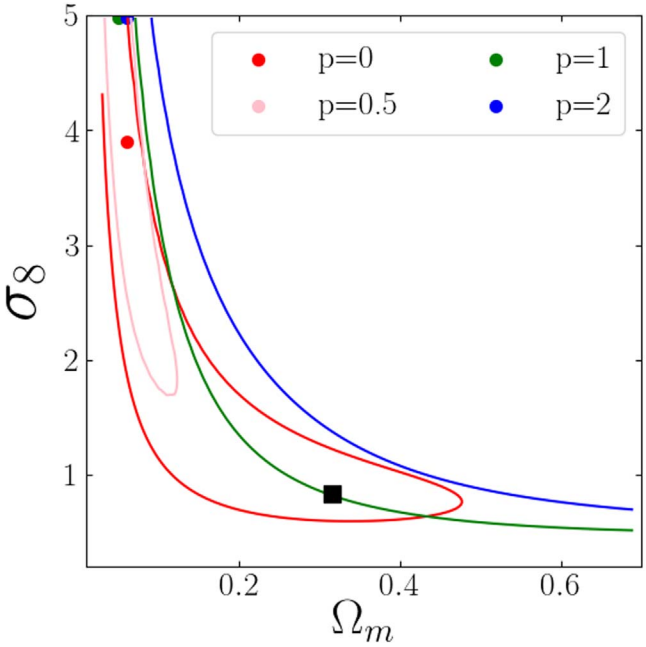

Figure 13. Ω_m and σ_8 constraints obtained from the CF3 galaxy survey using χ^2_t with the covariance matrix calculated using mock LG catalogs. The contours indicate the 68% likelihood values. The square marker indicates the best value from Planck (Planck Collaboration et al. 2014).

should allow us to use peculiar velocity correlations to place significant constraints on the cosmological parameters.

The χ^2_t is the appropriate one to use for real data, as it accounts for both cosmic variance and measurement errors. In Figure 13 we show the constraining result obtained by applying our method to the CF3 galaxy survey. In our calculations, we used the covariance matrix calculated from mock catalogs of LG observers with 20% distance uncertainties; this covariance matrix should be the best match to the cosmic variance and measurement uncertainties of the real data. In the figure, the observation constraining results agree with Planck (Planck Collaboration et al. 2014) within 1σ, except for $p = 0.5$. However, as expected the constraining contour is wide and flat and thus does not constrain the values significantly. In order to put tighter constraints on the cosmological parameters we require larger and/or more precise peculiar velocity surveys.

We also tested $f\sigma_8$ constraints for the CF3 galaxy survey and found no improvements. Furthermore, the $f\sigma_8$ statistic is an approximation that may lead to loss of information. In Figure 7, the bias caused by LG observers is mainly represented in the shape of the correlation function rather than of its magnitude. The shape of the linear-predicted correlation function is determined by the integral of the power spectrum (Equation (12)), which requires the value of Ω_m. Constraining $f\sigma_8$ requires a fixed Ω_m value for the power spectrum, which leads to a fixed shape of the correlation function. This would defeat our purpose of reducing the bias caused by LG observers, since the bias is mainly represented by the shape of the correlation function.

7. Conclusion

Previous studies of velocity correlations have mostly focused on ψ_1, a correlation function introduced by Gorski (Gorski 1988). This function has several disadvantages. First, it is dependent on the distribution of objects being analyzed and hence is not comparable between surveys. Second, it is a complicated mixture of physically meaningful correlation functions that quantify the correlations of velocity components parallel and perpendicular to the separation vector between pairs of galaxies. Third, as shown by Wang et al. (2018), the distribution of cosmic variance in ψ_1 is significantly non-Gaussian, complicating its use as a cosmological probe. Finally, as noted by Hellwing et al. (2017), and as we have shown here, our special location near the Virgo Cluster can bias correlation functions calculated using typical catalogs, whose density of objects decreases rapidly with distance.

In this paper we have presented an alternative method, an extension of a method introduced by Kaiser (1989) and Groth et al. (1989), that can stably estimate the parallel and perpendicular correlation functions directly from currently available peculiar velocity data. We have shown that the non-Gaussian distribution of the cosmic variance in ψ_1 is mostly due to its containing $\Psi_\perp$; the parallel correlation function $\Psi_\parallel$ has a more Gaussian distribution and therefore should be much more useful as a cosmological statistic.

We have shown that parallel and perpendicular correlation functions calculated with uniform weights are biased in LG-centered mock catalogs, especially for small separations. The LG mock catalog results also show less agreement between the results of using estimators ($\Psi_\parallel$ and $\Psi_\perp$) and the results of using the full 3D velocity fields ($\Psi_\parallel^{3D}$ and $\Psi_\perp^{3D}$). $\Psi_\perp$ shows more bias, which explains the different behaviors shown by ψ_1 and ψ_2 when LG-centered mock catalogs were used in Hellwing et al. (2017).

Our results, together with those of Hellwing et al. (2017), suggest that velocity correlation functions calculated from peculiar velocity data dominated by nearby galaxies will be biased due to our location near the Virgo Cluster. We have presented a novel way to reduce this bias by including position weights in our analysis. These weights reduce the emphasis on nearby galaxies, which are overrepresented in most catalogs. The weighted correlation functions probe a larger effective volume and thus give better agreement with linear theory. In particular, we have shown that the bias due to our location near the Virgo Cluster is reduced when weights are used. However, we find that there is a trade-off between decreasing cosmic variance and increasing measurement uncertainties. The optimal power to use will depend on the particular characteristics of the survey being analyzed.

We find that the position-weighted $\Psi_\parallel$ is a better cosmological probe than the previously used ψ_1 in that it has more Gaussian-distributed errors. While currently available peculiar velocity data is sufficient for calculating $\Psi_\parallel$ in the local universe, it does not allow us to put significant constraints on cosmological parameters. However, with larger and/or more accurate peculiar velocity surveys on the horizon, we expect velocity correlations to become an important cosmological probe.

H.A.F. and R.W. were partially supported by National Science Foundation grant AST-1907404. An award of computer time was provided by the INCITE program. R.W. and S.P. acknowledge support from the Murdock Charitable Trust College Research Program.

ORCID iDs

Yuyu Wang https://orcid.org/0000-0002-0245-8547
Richard Watkins https://orcid.org/0000-0001-7444-3216

References

Abate, A., & Erdoğdu, P. 2009, MNRAS, 400, 1541
Abate, A., & Feldman, H. A. 2012, MNRAS, 419, 3482
Agarwal, S., Feldman, H. A., & Watkins, R. 2012, MNRAS, 424, 2667
Bel, J., Pezzotta, A., Carbone, C., Sefusatti, E., & Guzzo, L. 2019, A&A, 622, A109
Bernardi, M., Alonso, M. V., da Costa, L. N., et al. 2002, AJ, 123, 2990
Bianchi, D., Percival, W. J., & Bel, J. 2016, MNRAS, 463, 3783
Borgani, S., da Costa, L. N., Zehavi, I., et al. 2000, AJ, 119, 102
Colless, M., Saglia, R. P., Burstein, D., et al. 2001, MNRAS, 321, 277
da Costa, L. N., Bernardi, M., Alonso, M. V., et al. 2000, AJ, 120, 95
Dale, D. A., Giovanelli, R., Haynes, M. P., Campusano, L. E., & Hardy, E. 1999, AJ, 118, 1489
Davis, M., Nusser, A., Masters, K. L., et al. 2011, MNRAS, 413, 2906
Dolag, K., Hansen, F. K., Roncarelli, M., & Moscardini, L. 2005, MNRAS, 363, 29
Dolag, K., Komatsu, E., & Sunyaev, R. 2016, MNRAS, 463, 1797
Dupuy, A., Courtois, H. M., & Kubik, B. 2019, MNRAS, 486, 440
Eisenstein, D. J., & Hu, W. 1998, ApJ, 496, 605
Feldman, H., Juszkiewicz, R., Ferreira, P., et al. 2003, ApJL, 596, L131
Feldman, H. A., Watkins, R., & Hudson, M. J. 2010, MNRAS, 407, 2328
Ferreira, P. G., Juszkiewicz, R., Feldman, H. A., Davis, M., & Jaffe, A. H. 1999, ApJL, 515, L1
Giovanelli, R., Haynes, M. P., Salzer, J. J., et al. 1998, AJ, 116, 2632
Gorski, K. 1988, ApJL, 332, L7
Gorski, K. M., Davis, M., Strauss, M. A., White, S. D. M., & Yahil, A. 1989, ApJ, 344, 1
Groth, E. J., Juszkiewicz, R., & Ostriker, J. P. 1989, ApJ, 346, 558
Habib, S., Pope, A., Finkel, H., et al. 2016, NewA, 42, 49
Hand, N., Addison, G. E., Aubourg, E., et al. 2012, PhRvL, 109, 041101
Hand, N., Seljak, U., Beutler, F., & Vlah, Z. 2017, JCAP, 10, 009
Heitmann, K., Finkel, H., Pope, A., et al. 2019a, ApJS, 245, 16
Heitmann, K., Uram, T. D., Finkel, H., et al. 2019b, ApJS, 244, 17
Hellwing, W. A. 2014, arXiv:1412.8738
Hellwing, W. A., Nusser, A., Feix, M., & Bilicki, M. 2017, MNRAS, 467, 2787
Hoffman, Y., Nusser, A., Courtois, H. M., & Tully, R. B. 2016, MNRAS, 461, 4176
Howlett, C., Staveley-Smith, L., & Blake, C. 2017, MNRAS, 464, 2517
Hudson, M. J., Smith, R. J., Lucey, J. R., & Branchini, E. 2004, MNRAS, 352, 61
Hudson, M. J., Smith, R. J., Lucey, J. R., Schlegel, D. J., & Davies, R. L. 1999, ApJL, 512, L79
Jaffe, A. H., & Kaiser, N. 1995, ApJ, 455, 26
Johnson, A., Blake, C., Koda, J., et al. 2014, MNRAS, 444, 3926
Juszkiewicz, R., Ferreira, P. G., Feldman, H. A., Jaffe, A. H., & Davis, M. 2000, Sci, 287, 109
Kaiser, N. 1987, MNRAS, 227, 1
Kaiser, N. 1988, MNRAS, 231, 149
Kaiser, N. 1989, in Large Scale Structure and Motions in the Universe, Astrophysics and Space Science Library, Vol. 151, ed. M. Mezzetti (Berlin: Springer), 197
Kashlinsky, A., Atrio-Barandela, F., Kocevski, D., & Ebeling, H. 2008, ApJL, 686, L49
Kumar, A., Wang, Y., Feldman, H. A., & Watkins, R. 2015, arXiv:1512.08800
Larson, D., Dunkley, J., Hinshaw, G., et al. 2011, ApJS, 192, 16
Linder, E. V. 2005, PhRvD, 72, 043529
Macaulay, E., Feldman, H., Ferreira, P. G., Hudson, M. J., & Watkins, R. 2011, MNRAS, 414, 621
Macaulay, E., Feldman, H. A., Ferreira, P. G., et al. 2012, MNRAS, 425, 1709
Masters, K. L., Springob, C. M., Haynes, M. P., & Giovanelli, R. 2006, ApJ, 653, 861
Melott, A. L., Coles, P., Feldman, H. A., & Wilhite, B. 1998, ApJ, 496, L85
Nusser, A. 2014, ApJ, 795, 3
Nusser, A. 2016, MNRAS, 455, 178
Nusser, A., Branchini, E., & Davis, M. 2011, ApJ, 735, 77
Nusser, A., & Davis, M. 2011, ApJ, 736, 93
Okumura, T., Hand, N., Seljak, U., Vlah, Z., & Desjacques, V. 2015, PhRvD, 92, 103516
Okumura, T., Seljak, U., Vlah, Z., & Desjacques, V. 2014, JCAP, 5, 003
Planck Collaboration, Ade, P. A. R., Aghanim, N., et al. 2014, A&A, 571, A16
Planck Collaboration, Ade, P. A. R., Aghanim, N., et al. 2016, A&A, 586, A140
Planck Collaboration, Aghanim, N., & Akrami, Y. 2020, A&A, 641, A6
Reid, B. A., & White, M. 2011, MNRAS, 417, 1913
Scoccimarro, R. 2004, PhRvD, 70, 083007
Scrimgeour, M. I., Davis, T. M., Blake, C., et al. 2016, MNRAS, 455, 386
Seiler, J., & Parkinson, D. 2016, MNRAS, 462, 75
Seljak, U., & McDonald, P. 2011, Journal of Cosmology and Astro-Particle Physics, 11, 039
Senatore, L., & Zaldarriaga, M. 2014, arXiv:1409.1225
Song, Y.-S., Nishimichi, T., Taruya, A., & Kayo, I. 2013, PhRvD, 87, 123510
Springob, C. M., Magoulas, C., Colless, M., et al. 2014, MNRAS, 445, 2677
Springob, C. M., Masters, K. L., Haynes, M. P., Giovanelli, R., & Marinoni, C. 2007, ApJS, 172, 599
Springob, C. M., Masters, K. L., Haynes, M. P., Giovanelli, R., & Marinoni, C. 2009, ApJS, 182, 474
Sunyaev, R. A., & Zeldovich, I. B. 1980, MNRAS, 190, 413
Taruya, A., Nishimichi, T., & Bernardeau, F. 2013, PhRvD, 87, 083509
Taruya, A., Nishimichi, T., & Saito, S. 2010, PhRvD, 82, 063522
Thomas, B. C., Melott, A. L., Feldman, H. A., & Shandarin, S. F. 2004, ApJ, 601, 28
Tonry, J. L., Dressler, A., Blakeslee, J. P., et al. 2001, ApJ, 546, 681
Tonry, J. L., Schmidt, B. P., Barris, B., et al. 2003, ApJ, 594, 1
Tully, R. B., Courtois, H. M., Dolphin, A. E., et al. 2013, AJ, 146, 86
Tully, R. B., Courtois, H. M., & Sorce, J. G. 2016, AJ, 152, 50
Turnbull, S. J., Hudson, M. J., Feldman, H. A., et al. 2012, MNRAS, 420, 447
Uhlemann, C., & Kopp, M. 2015, PhRvD, 91, 084010
Vlah, Z., Castorina, E., & White, M. 2016, JCAP, 12, 007
Wang, Y., Rooney, C., Feldman, H. A., & Watkins, R. 2018, MNRAS, 480, 5332
Watkins, R., & Feldman, H. A. 2007, MNRAS, 379, 343
Watkins, R., & Feldman, H. A. 2015, MNRAS, 450, 1868
Watkins, R., Feldman, H. A., & Hudson, M. J. 2009, MNRAS, 392, 743
Wegner, G., Bernardi, M., Willmer, C. N. A., et al. 2003, AJ, 126, 2268
Willick, J. A. 1999, ApJ, 516, 47
Zaroubi, S., Zehavi, I., Dekel, A., Hoffman, Y., & Kolatt, T. 1997, ApJ, 486, 21
Zhang, P., Pan, J., & Zheng, Y. 2013, PhRvD, 87, 063526
Zheng, Y., Zhang, P., Jing, Y., Lin, W., & Pan, J. 2013, PhRvD, 88, 103510